PHILOSOPHICAL TRANSACTIONS OF THE ROYAL SOCIETY B BIOLOGICAL SCIENCES

Application of Optical Diffraction to Helical Structures in the Bacteriophage Tail

M. F. Moody

Phil. Trans. R. Soc. Lond. B 1971 **261**, 181-195
doi: 10.1098/rstb.1971.0049

Phil. Trans. Roy. Soc. Lond. B. **261**, 181–195 (1971) [181]
Printed in Great Britain

Application of optical diffraction to helical structures in the bacteriophage tail

By M. F. Moody
The Rockefeller University, New York, N.Y. 10021, *U.S.A.*

[Plates 33 and 34]

First, a brief account is given of the principles underlying the use of the optical diffraction pattern of a perfectly helical particle to determine its helical lattice. The practical value and difficulties of this method are then revealed by a survey of its application to three different helical components of the T-even bacteriophage tail.

The analysis of the structure of contracted sheath is much facilitated by the existence of two kinds of particle (contracted sheath and polysheath) with apparently the same helical lattice. Polysheath yields excellent optical diffraction patterns, and contracted sheath (which does not) reveals directly the number of helices in one set (information unobtainable from polysheath).

The clear annuli of the extended sheath simplify the determination of all its structural parameters except for the number of helices in any set. For estimating this number, visual inspection is in one respect superior to optical diffraction, but an unambiguous solution has not hitherto been possible.

The helical structure of the core is so faint that optical diffraction is indispensable for obtaining reliable structural data. Even with this method, only one structural parameter has been determined so far: the core is composed of annuli whose spacing is apparently identical with that of the annuli of the extended sheath.

1. Introduction

This paper surveys the uses and limitations of optical diffraction in the analysis of electron micrographs of helical structures, using as examples three interrelated structures in the T-even bacteriophage tail.

The extended sheath (figure 1, plate 33) is a metastable structure that contracts irreversibly during infection of the bacterium, or upon treatment with a wide variety of substances (Brenner *et al.* 1959; Kozloff & Lute 1959). After contraction, the sheath has a different helical structure (figure 2, plate 33), and a study of the molecular mechanism of contraction must start by a determination of the helical structures of the extended and contracted sheaths. The third structure to be discussed is the core (also called the 'tube' or 'needle') (figure 1, plate 33). During assembly of the T4 tail, the extended sheath is formed around the core (King 1968) in a way that suggests bonding between the sheath and core subunits. If this bonding is precise and invariant, there should be a simple geometrical relation between the helical structures of the extended sheath and the core, whose structure should therefore be determined.

Helical structures of viruses have usually been determined by X-ray diffraction (see Finch & Holmes's (1967) review), but this requires a substantial preparation (some tens of milligrams) of purified particles, which must then be persuaded to assume a parallel orientation. Neither of these requirements is necessary in order to obtain electron micrographs of the particles, so there is a strong motivation to develop reliable methods for determining helical structures from micrographs. Unfortunately, high magnification micrographs are extremely noisy, and it is usually necessary to improve the signal:noise ratio by some method of averaging, that is, by making use of the large redundancy of a long helical particle. Because of the variability of micrographs, the number that must be analysed is often large, so it is necessary to process enormous quantities of optical data simply and quickly. Because of the present limitations of

computers and their ancillary equipment, these requirements are best satisfied by optical analogue devices, of which the most generally useful has proved to be the optical diffractometer (Taylor & Lipson 1964), first applied to electron micrographs by Klug & Berger (1964).

Before we describe how this method has been used in studying the structure of the phage tail, it will be useful to give a short account of the connexion between the optical transforms of perfectly helical particles and their structure.

2. Optical transforms of perfectly helical particles

A micrograph of a negatively stained particle gives some approximation to the projection of the density distribution of the surrounding stain. If the approximation were perfect, if the variations in the distribution of stain were entirely caused by the particle's structure, and if that structure were perfectly helical, then the micrograph's optical transform could be regarded as a plane section of the (three-dimensional) transform of a perfectly helical particle. This useful approximation will now be described, consideration of its deviations from reality being postponed to later sections.

The relation between the structure and transform of a helical particle is treated by helical diffraction theory (Cochran, Crick & Vand 1952; Klug, Crick & Wyckoff 1958). This theory performs for helical structures the service conventional diffraction theory performs for crystals: it views the structure as the superposition of a set of wave-like density distributions, each of which gives rise to a clearly identifiable part of the diffraction pattern. In the case of conventional diffraction theory, the density distributions are parallel planes of sinusoidally varying density, and each set of planes gives rise to just one pair of points in the transform of a crystal. In the same way, one can consider a helical structure as the superposition of coaxial thin cylindrical shells each consisting of a set of sinusoidal waves of density, following the path of n parallel helices of pitch P. Figure 3*a* shows such a structure, viewed in projection from the side (like a helical particle in a micrograph); its transform amplitude is shown in figure 3*b*. Ignoring the part† along the ξ axis (which for various reasons is not used in practice), the transform is confined to two lines, $\zeta = \pm n/P$. Along each line it consists of two principal maxima, each flanked by several subsidiary ones. When n and P are both zero, the density waves are annular (figure 3*c*), and there is now only one (central) principal maximum along each line of the transform (figure 3*d*). Any helical structure can be represented as the sum of various component

† This part disappears if one uses density waves of alternating sign, which are more satisfactory mathematically, but cannot be represented adequately in a diagram like figure 3*a*.

Description of plate 33

(All micrographs negatively stained with uranyl acetate.)

Figure 1. T4 bacteriophage (right) with extended sheath (e.s.). On the left, a core, attached to a base-plate at the right-hand end. (Magn. × 200 000.)

Figure 2. A T4 particle whose sheath has contracted after detaching from the base-plate (bottom). (During infection these two structures remain attached.) Helices of sets 1 and 2 are indicated on the contracted sheath. (Magn. × 390 000).

Figure 4. T4 contracted sheaths standing on end in a shallow layer of negative stain. The helices of set 1 (figure 2, above) appear as spiral projections which, in the left-hand sheath, clearly number 12. (Magn. × 330 000).

Figure 5. Part of a long piece of T4 polysheath which is partly disintegrated at the right, where it apparently connects with the short segment of contracted sheath or polysheath at the neck of the phage particle. (Magn. × 290 000.)

PHILOSOPHICAL TRANSACTIONS OF THE ROYAL SOCIETY B BIOLOGICAL SCIENCES

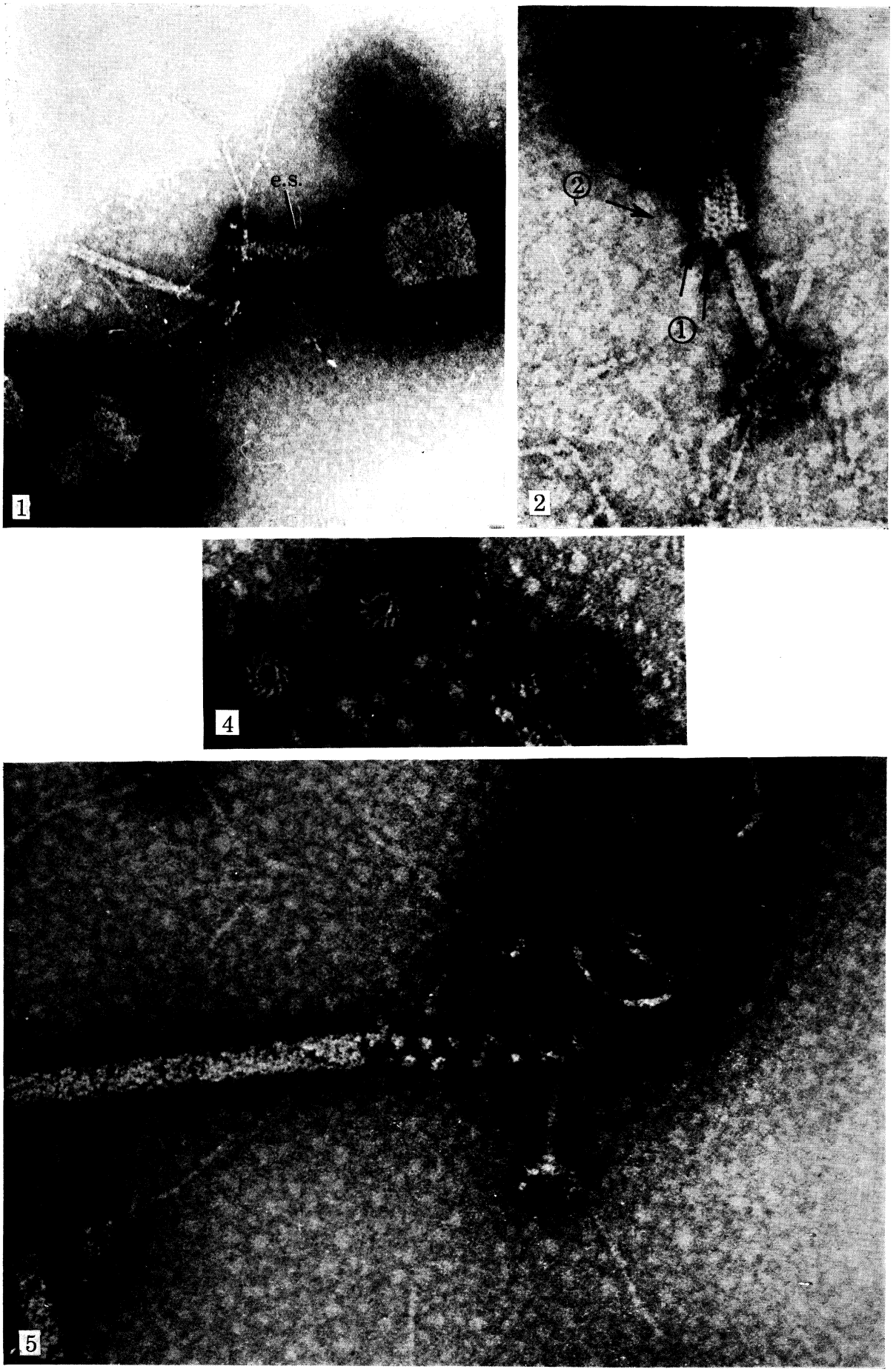

FIGURES 1, 2, 4 and 5. For legends see facing page.

(*Facing p.* 182)

PHILOSOPHICAL TRANSACTIONS OF THE ROYAL SOCIETY B BIOLOGICAL SCIENCES

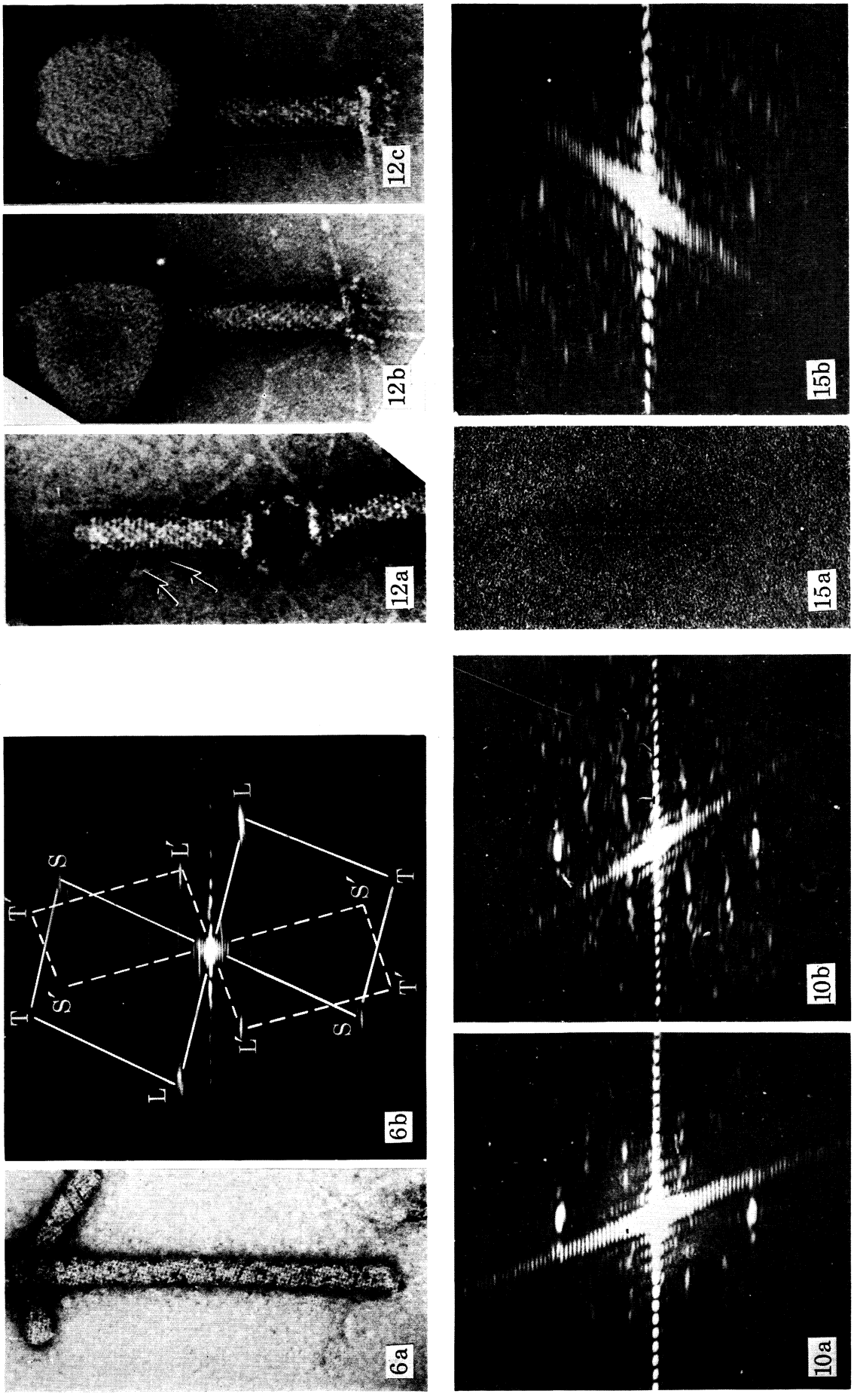

FIGURES 6, 10, 12 and 15. For legends see facing page.

PHILOSOPHICAL TRANSACTIONS OF THE ROYAL SOCIETY B BIOLOGICAL SCIENCES

density distributions† like figures 3*a* and 3*c*, each with appropriate amplitudes and values of *n* and *P* (or, if annular, of *m* and *h*) and *r*. The helical structure's transform will consist of the sum of the corresponding transforms, due attention being paid to their phases (not shown in figures 3*b* and 3*d*).

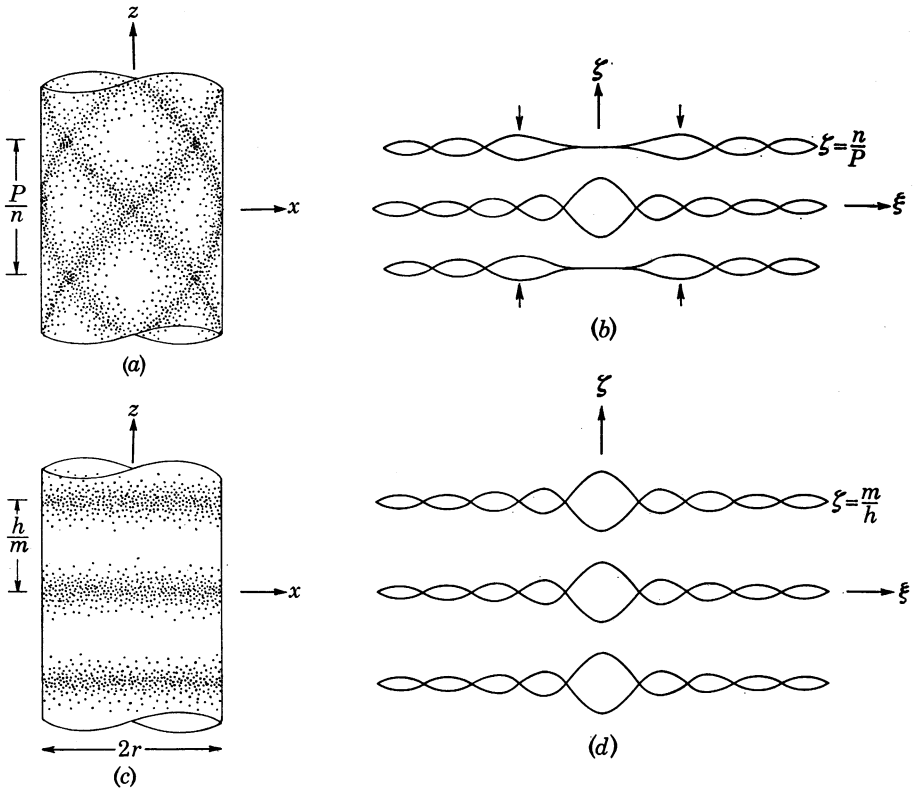

FIGURE 3. (*a*) Thin cylindrical shell, consisting of a set of sinusoidal waves of density, viewed in projection in the *xz* plane. The density waves follow the paths of helices, *n* in number and of pitch *P* ($n = 4$ in this diagram). (*b*) Transform amplitude of (*a*) in the (reciprocal) $\xi\zeta$ plane. The precise amplitude distribution depends on *n*, and ξ_M—the ξ coordinate of the principal maximum (arrowed)—is roughly proportional to *n* (for given *r*). (*c*) Thin cylindrical shell consisting of a set of annular sinusoidal waves of density, with axial periodicity *h*/*m*. (*d*) Transform amplitude of (*c*) (*m* does not affect the amplitude distribution (for given *r*)—only the separation of the layer lines).

† Correct adjustment of the background level of the helical structure requires, in addition, uniform cylinders of various radii and amplitudes; but these affect only the ξ axis of the transform.

DESCRIPTION OF PLATE 34

FIGURE 6. (*a*) Specimen of T4 polysheath embedded in a shallow layer of negative stain. (Magn. × 210 000). (*b*) Optical diffraction pattern of (*a*). The horizontal line (or 'spike') of bright spots marks the ξ axis. Diffraction spots deriving from the more prominent surface of the polysheath are joined with continuous lines and marked with unprimed capitals; those relating to the other side are joined with broken lines and marked with primed capitals. (5.2 cm correspond to 1 cm^{-1} of *a*.)

FIGURE 10. Optical diffraction patterns of T2L extended sheaths. Lettering of the layer lines indicates the corresponding points in the (n, ζ) diagram (figure 11). (1 cm ≡ 0.14 nm^{-1}.)

FIGURE 12. T4 extended sheaths, showing the annuli (24 narrow, light, horizontal bands) and 'coarse' helices (arrowed in *a*). (*a*) shows predominantly one surface, particularly at the top. (Magn. × 270 000.)

FIGURE 15. (*a*) T2L core particle (see text) showing faint striations perpendicular to its axis. (Magn. × 240 000.) (*b*) Optical diffraction pattern of (*a*). (1 cm ≡ 0.13 nm^{-1}.)

(*a*) *Structure confined to a thin cylindrical surface*

The value of considering a helical structure as the sum of these particular density distributions is that we need relatively few of them. This is particularly true when the helical structure is confined to a thin cylindrical surface. Since the radius is constant, the component density distributions differ only in n, P (or m, h). If the helical structure is also of low resolution (like most micrographs), then few of these density distributions are required to approximate it. Its optical transform therefore consists of only a few components like figures 3*b* and *d*. Unless the helical particle has a very short repeat, each of these transform components has a different ζ coordinate, so they cannot interfere. In this simple case, then, each pair of layer lines of the transform corresponds to a single helical or annular density distribution, with characteristic n and P (or m and h) and with the same radius r.

In analysing the optical diffraction pattern, our task is to determine these parameters for each pair of layer lines. Since $\zeta = m/h (n = 0)$ or $= n/P$ $(n \neq 0)$, it is sufficient to determine n and ζ. The ζ coordinate is measured directly, but n must be inferred from the distribution of intensity along the ξ coordinate of the layer line. It is easy to see if n is zero, since there is then only one principal maximum, coincident with the ζ axis (figure 3*d*). If it is not zero, n must be found from measurements of the intensity distribution. For example, if the radius r of the helix is known, we need only measure the ξ coordinates of the principal maxima (denoted by ξ_M); then $2\pi r_M$ must be 1.84 if $n = 1$, 3.05 if $n = 2$, etc. Values up to $n = 14$ are tabulated in Moody (1967*a*, p. 193); they are simply the values of the argument at the first maximum of the Bessel function of order n. If r were not known, both r and n could be inferred (for a helical structure confined to a thin cylindrical shell) since the intensity distribution must be $J_n^2(2\pi r\xi)$.

Having found n and ζ for any pair of layer lines, we mark points at either $\pm(n, \zeta)$ or $\pm(n, -\zeta)$ in an (n, ζ) plot† (examples are shown in figures 7 and 11), choosing the alternatives (see p. 185) so that all the points form a lattice. From the lattice of the (n, ζ) plot we can calculate the lattice of the helical surface. For, if that surface were cut parallel to the axis and opened flat, we should have a long flat sheet (of width $2\pi r$) in which the component annuli or helices would appear as parallel, equidistant, straight bands of density. Two adjacent bands would intersect the cut edge (parallel to the helix axis) with a separation of $1/\zeta$ (measured peak-to-peak), and they would intersect any perpendicular line with a separation of $2\pi r/n$. This is entirely analogous to the way in which the parallel straight bands of density in the (001) projection of a crystal intersect the axes with separations of a/h and b/k. Just as each set of bands with indices h and k corresponds to two points (h, k) and $(\bar{h}, \bar{k})$ in the $hk0$ plane of the reciprocal lattice, so the bands with indices n and ζ correspond to two points (n, ζ) and $(-n, -\zeta)$ in the (n, ζ) plot. (The only difference is that ζ, unlike k, is continuously variable, since the helix is not required to have an exact repeat along its axis.) Continuing the analogy, the construction of an (n, ζ) plot corresponds to the indexing of the diffraction patterns of a crystal, and the calculation of the helical lattice from the (n, ζ) plot is as straightforward as the calculation of unit cell dimensions from a known reciprocal lattice.

The analogy between space lattices and helical lattices goes even further. Just as a crystal usually possesses rotational (etc.) symmetry in addition to the translational symmetry of its space lattice, so a helical particle may possess dyads perpendicular to its long axis, in addition to

† The (n, ζ) plot (Moody 1967*a*) is a more convenient version of the closely related (n, l) plot (Klug *et al.* 1958).

the symmetry implied by the helical lattice. We therefore need to know whether or not the particle is *polar*. There is also another point to be decided. A helical lattice (unlike a space lattice) is usually enantiomorphous, and further evidence is needed to determine the choice of *hand*. The optical diffraction pattern could help us to obtain evidence concerning handedness, since this evidence often depends on the detection of minor departures from mirror symmetry due to tilting, shadowing or anisotropic contraction of the particle. But the centrosymmetry of an optical diffraction pattern renders it useless in deciding whether or not the particle is polar.

(*b*) *Structure at different radii*

When the helical structure is not confined to a single cylindrical surface, it is more difficult to determine the helical lattice from optical transforms. This is because the structure usually requires not just one set of helices of given number and pitch, but several equivalent sets, with the same number and pitch, but with different radii (and density). All these equivalent sets, having the same n/P, give optical transforms which lie along the same layer lines, and which therefore interfere. When n is more than zero, interference can substantially displace the position and height of the principal maxima—indeed, there may be more than two 'principal' maxima on the layer line. In these circumstances the estimation of n is subject to considerable uncertainty.

Nevertheless, it is usually possible to make a rough estimate of at least the relative values of n for the different layer lines. This information, combined with the precise values of the ζ coordinates of the layer lines, allows the corresponding (n, ζ) points to be arranged in their correct relative positions on a lattice, even though none of the n coordinates may be known with much accuracy. The construction of the (n, ζ) lattice is the first stage in the analysis of an optical diffraction pattern. However, the paucity of layer lines in some patterns can result in an ambiguity. From each layer line one measures or estimates $|n|$ and $|\zeta|$, and places two points at either $\pm(|n|, |\zeta|)$ or $\pm|(n|, -|\zeta|)$. These alternatives differ if n is not zero. For the first two points on the (n, ζ) plot, the choice is unimportant,† but for the second pair of points it determines the unit cell of the (n, ζ) lattice. If no further points (i.e. no further layer lines) are available, we have an ambiguity concerning the shape of the (n, ζ) (and consequently of the helical) lattice. (In practice, this ambiguity can sometimes be eliminated if the staining conditions are very different on the upper and lower surfaces of the particle; see figure 6*b*, plate 34.) But if further points *are* available, their coordinates will prove consistent with only one of the alternative lattices. Consequently the determination of the correct unit cell of the lattice requires at least three pairs of non-meridional layer lines, but only two pairs if one of the pairs has meridional diffraction spots.

Although none of the n-coordinates may be known with certainty, the construction of an approximate (n, ζ) lattice reduces the number of unknowns to two n coordinates (since the lattice is completely determined by two basic (n, ζ) vectors). Moreover, the permissible ranges of these two n-values are limited by the combined information from the entire optical diffraction pattern. Consequently, although the optical transform of a thick helix does not generally give a unique solution to the helical lattice, it does yield a reasonably small number of alternative solutions between which it may be possible to decide on other grounds.

† It determines the enantiomorph of the (n, ζ) lattice. Since the handedness of the helical lattice is rarely (if ever) determined from the optical diffraction pattern alone, it is necessary to ignore such questions during its analysis.

PHILOSOPHICAL TRANSACTIONS OF THE ROYAL SOCIETY B BIOLOGICAL SCIENCES

3. Contracted sheath and polysheath

Of the three tail structures mentioned in § 1, we start by considering the one for which optical diffraction proved most satisfactory. Paradoxically, the contracted sheath itself gives very poor optical diffraction patterns (see Plate IX of Moody 1967*a*). This is partly due to the relatively small number of repeating units (144); but the extended sheath, with the same number, gives much better patterns. Probably the main cause is the stubby shape of the contracted sheath

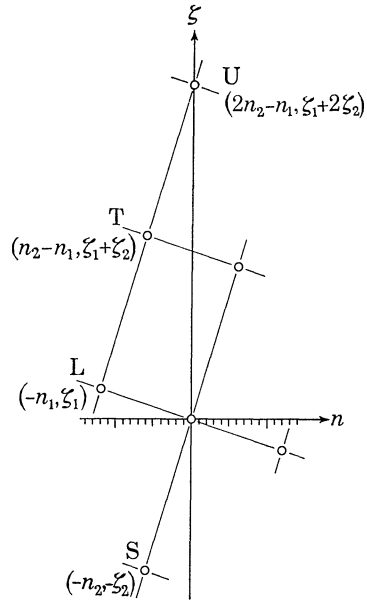

Figure 7. (n, ζ) plot of polysheath and contracted sheath.

(figure 2, plate 33), allowing it to be misalined and distorted on the electron microscope grid. However, this property actually proved an advantage, for it allows the sheath to stand on end without bending when the negative stain is dried. This stain (uranyl acetate) contracts during drying and exposure to the electron beam—a fact that can be abundantly verified by observing the bizarre distortions sometimes seen in particles suspended in stain over holes in the supporting film. The effect of this contraction is to reduce the diameter of the projecting end of a contracted sheath, but not of the end adhering to the film. The sheath particle thus becomes conical (Moody 1967*a*) and, when viewed down its axis, a set of helices of long pitch (set 1 in figure 2, plate 33) can be seen in spirals of which there are clearly 12 (figure 4, plate 33).

The unsuitability of contracted sheath for optical diffraction was compensated for by the existence of a closely related, aberrant tail structure—polysheath (figure 5, plate 33) which apparently has the same helical symmetry (Kellenberger & Boy de la Tour 1964; Moody 1967*a*). Polysheath is almost ideal for optical diffraction: it is usually long and straight; and the negative stain does not penetrate far below its surface, so that the helical structure revealed in micrographs is apparently confined to a rather small range of radii. (This was of value in the calculation of the expected ξ_M values—see later.)

The first step in the analysis of an optical diffraction pattern is to construct an (n, ζ) plot with the relative n values qualitatively correct. For a layer-line at $\zeta = n/P$, the ξ coordinates of the principal maxima $(\xi_M(n))$ are roughly proportional to n, so that this preliminary (n, ζ) plot

can be indicated on the optical diffraction pattern itself (figure 6*b*, plate 34). When we construct from this the quantitatively correct (n, ζ) plot (figure 7), the only problem is to determine two n coordinates, for example n_1 and n_2. n_1 is (from the apparent identity of the helical lattices of polysheath and contracted sheath) the number of helices seen as spirals in figure 4, that is, $n_1 = 12$. Only n_2 remains to be determined from the different ξ_M values. The spots S and T (or S′ and T′) in figure 6*b*, plate 34, obviously have very similar ξ_M values, and these should be exactly the same if $n_2 = 6$, since the n coordinates of both S and T in the (n, ζ) plot (figure 7) would then be 6. To check whether this was so, it was necessary to calculate the ξ_M values expected for the nearest alternatives ($n_2 = 5$ or 7).

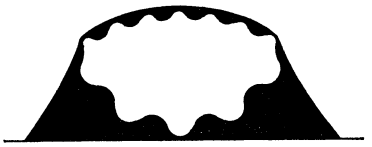

FIGURE 8. Hypothetical cross-section of a contracted sheath or polysheath, embedded in a shallow layer of negative stain (black). The upper part of the stain has suffered a contraction that flattens the top surface of the embedded particle.

Such a calculation is usually subject to substantial error. First there is the problem of how to determine the radial density distribution. This could fortunately be ignored in the case of polysheath, in which the helical structure revealed by negative stain appears to be confined essentially to one radius. Next there is the problem of measuring the radius; but this was circumvented by using the ratios of the ξ_M values for different layer lines, since different sets of helices fortunately have approximately the same radius. More serious is the problem of how accurately the image of a negatively stained helical particle represents the two-dimensional projection of its undistorted structure. In fact, the polysheath particles that were examined showed evidence of distortion which was greatest in the case of particles embedded in a shallow layer of negative stain. This evidence came from the departures from mirror symmetry in the corresponding optical diffraction patterns. For example, the principal maxima L and L′ in figure 6*b* are not true mirror images with respect to the horizontal 'spike'. The greater distance of the L maxima from the meridian is due to the contraction† of the upper (i.e. projecting) surface of the polysheath—an effect related to the contraction of the projecting end of a negatively stained contracted sheath (p. 186). Now, if the upper surface is to contract while remaining joined to an undistorted lower surface, the upper surface must also flatten (figure 8).

The effect of such distortions on the optical diffraction pattern was investigated (Moody 1967*a*, appendix 1). Provided they are uniform along the length of the particle, the distortions cannot change the ζ coordinates of the layer lines. (This uniformity can be checked, since any serious departure should cause splitting of the layer lines.) However, the ξ coordinates of the principal maxima (ξ_M) *are* dependent on the precise degree of flattening of each surface. Since this degree is usually unknown, the various extreme cases (in which each surface is either semi-circular or flat) were considered, and the corresponding ξ_M values were calculated for different numbers of helices.

Using the methods described in the previous two paragraphs, the ξ_M values were calculated

† Departures from mirror symmetry in the optical diffraction patterns of helical particles can also occur if the two surfaces are stained with different density. If this is the cause, the main effect is a difference in the intensity of the two principal maxima of a layer line, although slight movements of their position will also occur (Moody 1967*a*, appendix 1).

PHILOSOPHICAL TRANSACTIONS OF THE ROYAL SOCIETY B BIOLOGICAL SCIENCES

for $n_2 = 5$ or 7, and compared with the observed values (Moody 1967*a*, appendix 2). From the substantial discrepancy, it followed† that $n_2 = 6$. Since n_1 was known to be 12, this information determines the (n, ζ) plot of contracted sheath, and from this the helical lattice of contracted sheath was calculated (figure 9). However, the solution of this structure depended on two fortunate circumstances—direct evidence for one of the n coordinates, and the narrow range of radii contributing to the optical diffraction pattern—that are usually absent.

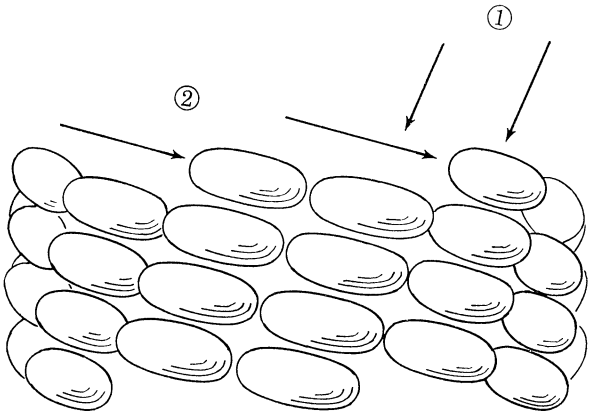

FIGURE 9. The arrangement of the outer parts of the subunits in one-third of a contracted sheath. Helices of sets 1 and 2 are indicated.

4. EXTENDED SHEATH

(*a*) *Structure determination by optical diffraction*

We start by deducing, as far as possible, the structure of the extended sheath from its optical transform (analysed by Krimm & Anderson (1967) and by DeRosier & Klug (1968)). Figure 10 (plate 34) shows two very prominent spots (A) which are clearly meridional. (The possibility that they represent non-meridional spots from a completely one-sided helix is clearly excluded since the other layer lines all contain *pairs* of spots. (For further discussion of this point see § 5, p. 192)). As was pointed out in § 2 (p. 184), this shows, independently of considerations of the particle's radius and shape, that the corresponding n coordinate is zero. The two meridional spots therefore correspond to the vector $(0, \zeta_0)$ of the (n, ζ) lattice (figure 11). Only one more point is required to fix the (n, ζ) lattice; consequently the correlation of the other layer lines (B, C, D, E in figure 10*a*), with the corresponding (n, ζ) points (figure 11) is relatively straightforward.

At this stage everything necessary to fix the (n, ζ) plot has been measured, with one exception: we need the exact value of any non-zero n coordinate. However, the determination of one of these coordinates from the intensity distribution on the corresponding layer lines is more difficult than it was in the case of polysheath.

† From this it also follows that the n coordinate of the point U in the (n, ζ) plot (figure 7) is zero, so that the corresponding layer line in the optical diffraction pattern should contain a single meridional maximum (instead of two maxima if $n_2 = 6$). This qualitative distinction would hold irrespective of the radius or shape of the particle, and would thus determine the structure simply and unambiguously. This layer line is visible in the diffraction pattern of extended sheath (the spot on line A in figure 10*a*, plate 34); but, after contraction of the sheath, it lies beyond the resolution of the negative staining technique.

The basic difficulty is that the helical structure of extended sheath is not confined to a single cylindrical surface. Instead, some of the extended sheath helices have their structure revealed at substantially different radii. This is particularly true of the helices indicated by arrows in figure 12*a*, plate 34. (These will be referred to as 'coarse' helices, following Daems, Van de Pol & Cohen (1961)). If the micrographs (especially figure 12*a*) are viewed at a glancing angle from a direction that gives a tangential view of the helices, the helices appear more broadened at the edges of the particle than at its centre. The same conclusion follows from the indexing of the optical diffraction pattern: both the spots E_1 and E_2 (figure 10*b*) must correspond to the same pair of points, $\pm(n_1, \zeta_1)$ in figure 11. E_1 and E_2 thus relate to helices which, having the

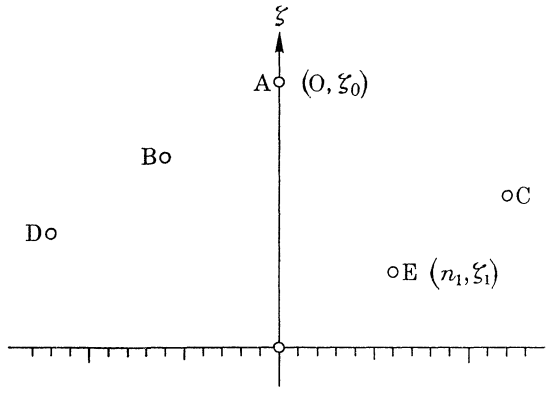

FIGURE 11. (n, ζ) plot for extended sheath. A, B, etc. indicate points corresponding to the layer lines marked in figure 10 (plate 34).

same number, sense and axial repeat, can differ only in radius. (A detailed picture of the radial density distribution of the different helices is obtainable by optical filtering or three-dimensional reconstruction (DeRosier & Klug 1968).)

As we saw in § 2, p. 185, this causes interference on the layer lines, making the ξ_M values untrustworthy for quantitative calculations of the corresponding n coordinates.† Consequently the optical diffraction analysis of extended sheath yields, not a unique structure, but rather a few alternative ones, with different values of n_1.

(*b*) *Structure determination without optical diffraction*

Independently of the optical diffraction study of extended sheath (Krimm & Anderson 1967), essentially the same structural conclusions were reached by direct examination and measurement of the micrographs (Moody 1967*b*). A comparison of the two approaches reveals some of the advantages and limitations of optical diffraction as a method for determining helical structures from micrographs. To facilitate this comparison, we now show how the (n, ζ) plot could be constructed point by point from identifiable features in the extended sheath (figure 12, plate 34).

The most obvious feature of the extended sheath is a set of 24 striations perpendicular to its axis. These are clearly separated from each other near the particle's axis, even in micrographs in

† Krimm & Anderson (1967) estimated the extended sheath radius (and hence n_1) from the positions of the subsidiary maxima surrounding the meridional spot on layer line A (figure 10). But (apart from the difficulty of measuring their positions accurately) this method is rendered inaccurate by ignorance of the precise density distribution of the different helices and annuli, in the same way as was the method based on ξ_M values.

which other helices are visible from both sides. The striations are therefore caused by annuli, and not by helices. It follows that the (n, ζ) plot (figure 11) has two points $(0, \pm\zeta_0)$, where ζ_0 is the reciprocal of the striation periodicity. The next most obvious feature of extended sheath is the set of 'coarse' helices (arrowed in figure 12*a*). These are sufficiently clear for their axial periodicity $(1/\zeta_1)$ to be measured. The number of these helices (n_1) can also be estimated by visual inspection, with an accuracy which is in one respect superior to that based on analysis of the optical diffraction pattern (see below). Given ζ_1 and an estimate of n_1, we add two more

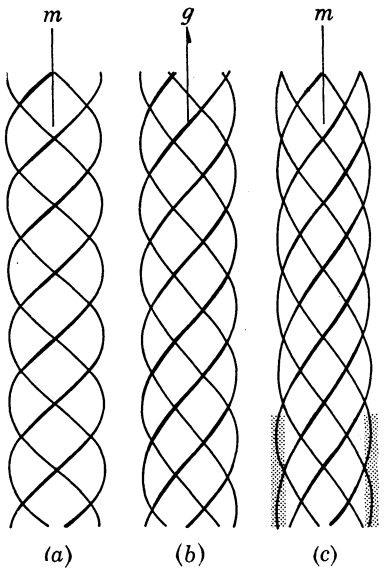

FIGURE 13. Appearance of different numbers of parallel helices (4 in *a*, 5 in *b* and 6 in *c*) in projection. When the number is even (*a*, *c*) the projection has a mirror plane (*m*), but otherwise (*b*) only a glide plane (*g*). The central part of (*c*) (that part at the bottom not covered by shading) has an appearance similar to (*a*), showing that a set of 6 helices may appear in micrographs as a set of four helices.

points at $\pm(n_1, \zeta_1)$ in the (n, ζ) plot (figure 11). We now have two independent vectors (with termini at points A and E of figure 11), which suffice to determine the (n, ζ) lattice of extended sheath.

It was possible to determine this lattice without the use of optical diffraction only because of two favourable circumstances. First, the striations (annuli) and the 'coarse' helices are sufficiently clear that their axial periodicities can be measured without the need for optical diffraction to minimize micrograph noise. Secondly, the existence of annuli allows the (n, ζ) lattice to be fixed (apart from its hand) by data from these annuli, and from only one set of helices. If no clear set of annuli had been visible, we should have had to measure the axial periodicities of at least *three* different sets of helices. It is most unusual for a micrograph to show so many helices with sufficient clarity for measurement; consequently an optical diffraction pattern is probably indispensable for analysing a particle which lacks clear annuli.

We now discuss the problem of finding n_1, the number of 'coarse' helices, by direct examination of these helices in micrographs (figure 12*b*, *c*) in which both surfaces are approximately equally stained, i.e. in which the lines curving from bottom left to top right are about as clear as those curving from bottom right to top left. In such micrographs the helices from the front surface appear related to those from the back by a mirror plane coincident with the particle's long axis. This shows that the number of 'coarse' helices is even (see figure 13). This important

information was missing from the optical diffraction pattern since it is contained in the *phase* of the spots along the layer lines deriving from the 'coarse' helices (E in figure 10*b*). Since the 'coarse' helices show a mirror plane in projection, the phases of the mirror-related points at (ξ, ζ_1) and $(-\xi, \zeta_1)$ should be equal. (If n_1 were odd, these phases would differ by 180°.) It is technically difficult to obtain the Fourier transform phases with an optical diffractometer; the most satisfactory method is to calculate them from the micrograph's optical density distribution. This was done by DeRosier & Klug (1968), and their results confirm that the phases of layer line E are related by a mirror plane (see figure 4, p. 131, of their paper).

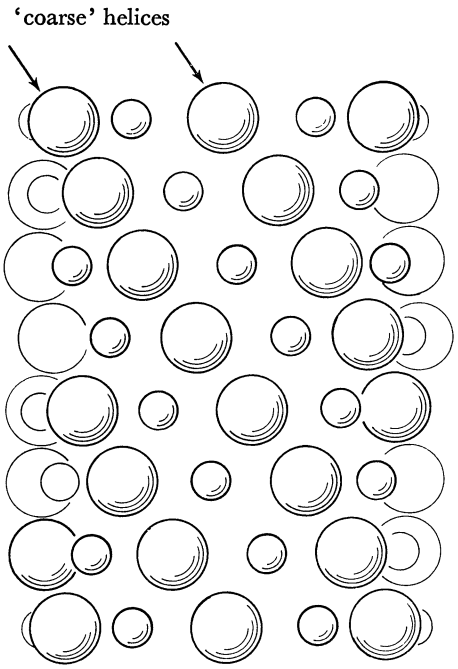

FIGURE 14. One-third of a T-even extended sheath, adopting the sixfold alternative for its rotation axis. (The hand is incorrect.) (The large and small subunits represent an approximation to the density distribution within the asymmetric unit.)

Unless phase information is available, it is therefore necessary to supplement the optical transform by further information from the micrographs. But, because of the noisiness of the micrographs, visual examination alone is not usually sufficient. However, it should be possible to have the best of both methods by the use of optical filtering to give clarified images of the different component helices of a structure, which are then examined visually for their symmetry, number and radial density distribution.

Returning to the extended sheath structure, we know that n_1 must be even. Further examination of the micrographs shows that n_1 cannot be less than 4 or greater than 6 (compare figure 12*b*, *c* with figure 13). This is probably the same range of values that would be given by a quantitative analysis of the optical diffraction pattern; but visual inspection eliminates, as we have seen, the possibility that $n_1 = 5$. Consequently n_1 must be 4 or 6. This is not only the number of 'coarse' helices, but also the order of the rotation axis of extended sheath.

PHILOSOPHICAL TRANSACTIONS OF THE ROYAL SOCIETY B BIOLOGICAL SCIENCES

(*c*) *Structure of extended sheath*

Neither optical diffraction, nor visual inspection, of the micrographs yields a unique structure for extended sheath: there are two alternative structures, depending on whether the order of the rotation axis is 4 or 6. The latter alternative (figure 14) is strongly supported by the structural relationships of the extended sheath (Moody 1967*b*), but it is unsatisfactory to have to rely on such evidence in a study from which conclusions are to be drawn about structural relationships. This difficulty in the determination of the number of helices in any set constitutes the main deficiency of present methods for determining helical structures from micrographs—see § 6.

The possible contraction mechanisms consistent with the known contracted sheath structure and the sixfold extended sheath structure have been discussed (Moody 1967*b*). More direct information about the correct mechanism is provided by studies of partially contracted sheaths, which will be published later.

5. Core

Micrographs of the core (figure 1) usually show it as a smooth, structureless hollow cylinder. However, cores sometimes appear to show faint striations perpendicular to their axes (figure 15*a*, plate 34). To decide whether this appearance is caused by regularly arranged structures, or is merely artefactual, it is necessary to use optical diffraction (or some other method) to improve the signal:noise ratio. The improvement is proportional to the length of the particle analysed. Fortunately, cores are naturally long ($\sim$ 100 nm), and even longer particles are readily produced by various treatments (Tikhonenko & Poglazov 1963; To, Kellenberger & Eisenstark 1969), presumably through partial reconstitution (perhaps from their subunits—Poglazov & Nikolskaya 1969).

From such cores (in a preparation of T2L ghosted by multiple freezing and thawing) preliminary structural data have been obtained. Optical diffraction patterns of these particles sometimes contained clear meridional reflexions (figure 15*b*). However, since the intensity of the background 'noise' peaks often approached that of the meridional spots, the reality of the latter was checked by measurements of their separation. This could be measured quite precisely in each case, and the measurements from different cores in the same micrograph were very similar (table 1), confirming the reality of the meridional reflexions. (A 'reflexion' spread over a range of distances from the origin of the diffraction pattern can result from defocus or astigmatism (Thon 1966). This possibility is excluded if the reflexions under consideration lie within the first dark ring (corresponding to spatial frequencies receiving a symmetrical phase of 180°, with respect to the spatial frequencies near the origin).)

Meridional reflexions almost always indicate the presence of annuli, but they can also be given by helices of small pitch if either of the two following conditions obtain. First, the particle's axis may be tilted so that it is no longer perpendicular to the optical axis of the microscope; however, this would not be possible with long core particles. Secondly, the particle may be stained effectively on only one surface. This possibility (which should give only a pseudo-meridional reflexion—see below) can usually be checked by studying other layer lines of the optical diffraction pattern. No other layer lines were visible in the patterns given by the core particles, but this possibility could be eliminated on other grounds. There is no known case of a narrow particle *never* staining on both surfaces, so a pseudo-meridional reflexion should at least occasionally appear split. This was never seen with the meridional reflexions of core.

PHILOSOPHICAL TRANSACTIONS OF THE ROYAL SOCIETY B BIOLOGICAL SCIENCES

Moreover, these reflexions were usually precisely meridional, whereas the pseudo-meridional reflexions of a particle consistently stained on only one surface should be always tilted away from the meridian (and always tilted in the same direction, if the particle were always stained on the same surface). For these reasons, the reflexions in the optical transform of core are believed to be truly meridional, showing that the core contains or consists of equally spaced annuli.

Since the extended sheath also consists of annuli, it is interesting to determine the relation between its annulus repeats and those of the core. This can be done accurately since there were, in the same micrographs, specimens of T2L extended sheath. Optical diffraction patterns were also taken of these, and the separation of the meridional spots is shown in table 2*a*. Table 2*b* shows the corresponding measurements for core (from table 1) divided by the average measurements for extended sheath (bottom of table 2*a*). These ratios can all be compared with each

TABLE 1. CORE SPACINGS

number of electron micrograph		
(i)	(ii)	(iii)
2.8	2.54	2.13
2.77	2.68	2.19
2.82	—	—

TABLE 2. COMPARISON OF CORE AND EXTENDED SHEATH

		number of electron micrograph		
		(i)	(ii)	(iii)
(*a*) extended sheath spacings		2.90	2.61	2.16
		2.77	2.76	2.18
		2.90	—	2.13
		2.86	—	2.15
		2.75	—	2.13
	mean	2.83	2.69	2.15
(*b*) $\frac{\text{core spacing}}{\text{mean extended sheath spacing}}$		0.99	0.95	0.99
		0.98	1.00	1.02
		1.00	—	—

Spacings measure separations of meridional spots in optical diffraction patterns (mm). (Spacings from different micrographs are not comparable, because of variations of magnification.)

other, even when they are obtained from different micrographs, and their agreement provides additional confirmation of the reality of the meridional spots. The average of all the ratios is 0.99 ± 0.02, and this is the average annulus repeat of extended sheath, divided by that of the core. In a complete extended sheath of 24 annuli, the number of core annuli in the same length is therefore $24\ (0.99 \pm 0.02) = 23.8 \pm 0.5$. Consequently the limited data available at present indicate that there is a one-to-one correspondence between the annuli of the core and of the extended sheath in T2L. The same correspondence has more recently been found in the completely unrelated *Subtilis* phage SP50 (F. Eiserling, personal communication), so it may be a general phenomenon of contractile phage sheaths.

Although it is perhaps possible that extended sheath and core independently have identical annulus spacings, it is more likely that the precise annulus spacing of extended sheath is determined by bonding between its annuli and those of the core. (As pointed out in § 1, the existence of such bonding is also implied by the way the length of the extended sheath is determined by the core.) However, the structure of incomplete extended sheaths (which are always continuous

PHILOSOPHICAL TRANSACTIONS OF THE ROYAL SOCIETY B BIOLOGICAL SCIENCES

down to the base-plate—King 1968), and the contraction process itself, indicate the presence of bonds between adjacent annuli of extended sheath. The extended sheath's final structure is presumably the result of a balance between these different bonds, so it will be interesting to see what relation (if any) its other helical parameters bear to those of the core.

6. Conclusions

An optical diffraction analysis naturally suffers from any defects in the electron micrograph image analysed. The most obvious deficiencies are the limitation of resolution (which is never much better than 2 nm in negatively stained preparations) and the lack of penetration of the negative stain into some important structural features of particles. The contraction of the stain also subjects the helical particle to distortions, of which some are known (see § 3, p. 186), but others may cause unsuspected errors. With the smallest structures, whose details approach the resolution limit of the technique, further problems may prove significant—for example the effects of irradiation and heating in causing submicroscopic changes in the structure of the stain, and also the effects of imaging defects and aberrations. In consequence, the reliability of the optical diffraction method will become established only when several helical structures have been determined both from electron micrographs and by the more reliable X-ray methods. It is hoped that this will prove possible in the case of some of the phage tail components discussed in this paper.

Apart from the question of its reliability, however, the optical diffraction method has one serious deficiency. In the preceding sections we have often encountered the problem of finding the number of helices in any particular set, especially when (as in the case of extended sheath) the helical particle has its structure revealed at several different radii. At present there is only one reliable method—the direct counting of the helices from a micrograph in which they are not superposed on each other. But the avoidance of superposition in negatively stained preparations requires extremely short fragments viewed end-on, and such micrographs are difficult to obtain from particles sufficiently long to give satisfactory optical diffraction patterns. There is therefore the need of a more general method for counting helices.

The first possibility to examine is whether or not the number of helices can be determined from a single projection perpendicular to the axis of a helical particle. We have seen that such a projection allows the possible helical lattices to be restricted to a small number of alternatives. It seems plausible that a more refined treatment, using calculated transforms which preserve the phases, might yield a unique solution to the problem, at least when the number of helices is not too large. Perhaps one might try to determine directly which order(s) of Bessel function is appropriate to each layer line. Unfortunately the orthogonality relations involving Bessel functions of different orders are complicated (Watson 1958, chapter XIII), and it is not clear whether this procedure would be mathematically possible, quite apart from the question of its feasibility when applied to actual micrographs. Alternatively, an attempt at three-dimensional reconstruction (De Rosier & Klug 1968) should lead to some inconsistency or absurdity (such as extensive regions of negative density) if the wrong helical lattice were used. It is hoped that this method will be tested, particularly in cases where the correct number of helices is already established.

Perhaps the most direct way to count helices would be to rotate the particle about its axis by successive known angular increments. The resulting set of stereo-micrographs, if obtained

from a perfectly helical particle, would certainly contain sufficient data to count all the sets of helices. The particles may have unsuspected distortions (perhaps along directions perpendicular to the supporting film) that would complicate the analysis. But the main difficulties are purely technical, deriving from the vibration sensitivity of tilting stages, the limitations imposed on them by the simultaneous operation of an anti-contamination device, and the familiar problem of radiation damage.

In conclusion, the optical diffraction method has greatly improved the reliability with which helical structures can be determined from electron micrographs. The method could be improved further, in particular by making use of the phases, as well as the intensities, of the transform. But we are already in a position where the greatest need is for improvements in the micrographs themselves.

I wish to thank Miss Jacqueline Lanoix for technical assistance, and Mr Tiden and the staff of the Instrument Shop for constructing the optical diffractometer. The work was supported by a grant (AI 07824) from the National Institutes of Health.

References (Moody)

Brenner, S., Streisinger, G., Horne, R. W., Champe, S. P., Barnett, L., Benzer, S. & Rees, M. W. 1959 *J. molec. Biol.* **1**, 281–292.
Cochran, W., Crick, F. H. C. & Vand, V. 1952 *Acta Crystallogr.* **5**, 581–586.
Daems, W. Th., Van de Pol, J. H. & Cohen, J. A. 1961 *J. molec. Biol.* **3**, 225–227.
DeRosier, D. J. & Klug, A. 1968 *Nature, Lond.* **217**, 130–134.
Finch, J. T. & Holmes, K. C. 1967 *Methods in virology* (eds. K. Maramorosch and H. Koprowski), vol. III, pp. 351–474. New York: Academic Press.
Kellenberger, E. & Boy de la Tour, E. 1964 *J. ultrastruct. Res.* **11**, 545–563.
King, J. 1968 *J. molec. Biol.* **32**, 231–262.
Klug, A. & Berger, J. E. 1964 *J. molec. Biol.* **10**, 565–569.
Klug, A., Crick, F. H. C. & Wyckoff, H. W. 1958 *Acta Crystallogr.* **11**, 199–213.
Kozloff, L. M. & Lute, M. 1959 *J. biol. Chem.* **234**, 539–546.
Krimm, S. & Anderson, T. F. 1967 *J. molec. Biol.* **27**, 197–202.
Moody, M. F. 1967*a* *J. molec. Biol.* **25**, 167–200.
Moody, M. F. 1967*b* *J. molec. Biol.* **25**, 201–208.
Poglazov, B. F. & Nikolskaya, T. I. 1969 *J. molec. Biol.* **43**, 231–233.
Taylor, C. A. & Lipson, H. 1964 *Optical transforms, their preparation and application to X-ray diffraction problems.* London: G. Bell and Sons Ltd.
Thon, F. 1966 *Z. Naturf.* **21**A, 476–478.
Tikhonenko, A. S. & Poglazov, B. F. 1963 *Biokhimiya* **28**, 274–279.
To, C. M., Kellenberger, E. & Eisenstark, A. 1969 *J. molec. Biol.* **46**, 493–512.
Watson, G. N. 1958 *A treatise on the theory of Bessel functions*, 2nd ed. Cambridge University Press.

PHILOSOPHICAL TRANSACTIONS OF THE ROYAL SOCIETY B BIOLOGICAL SCIENCES

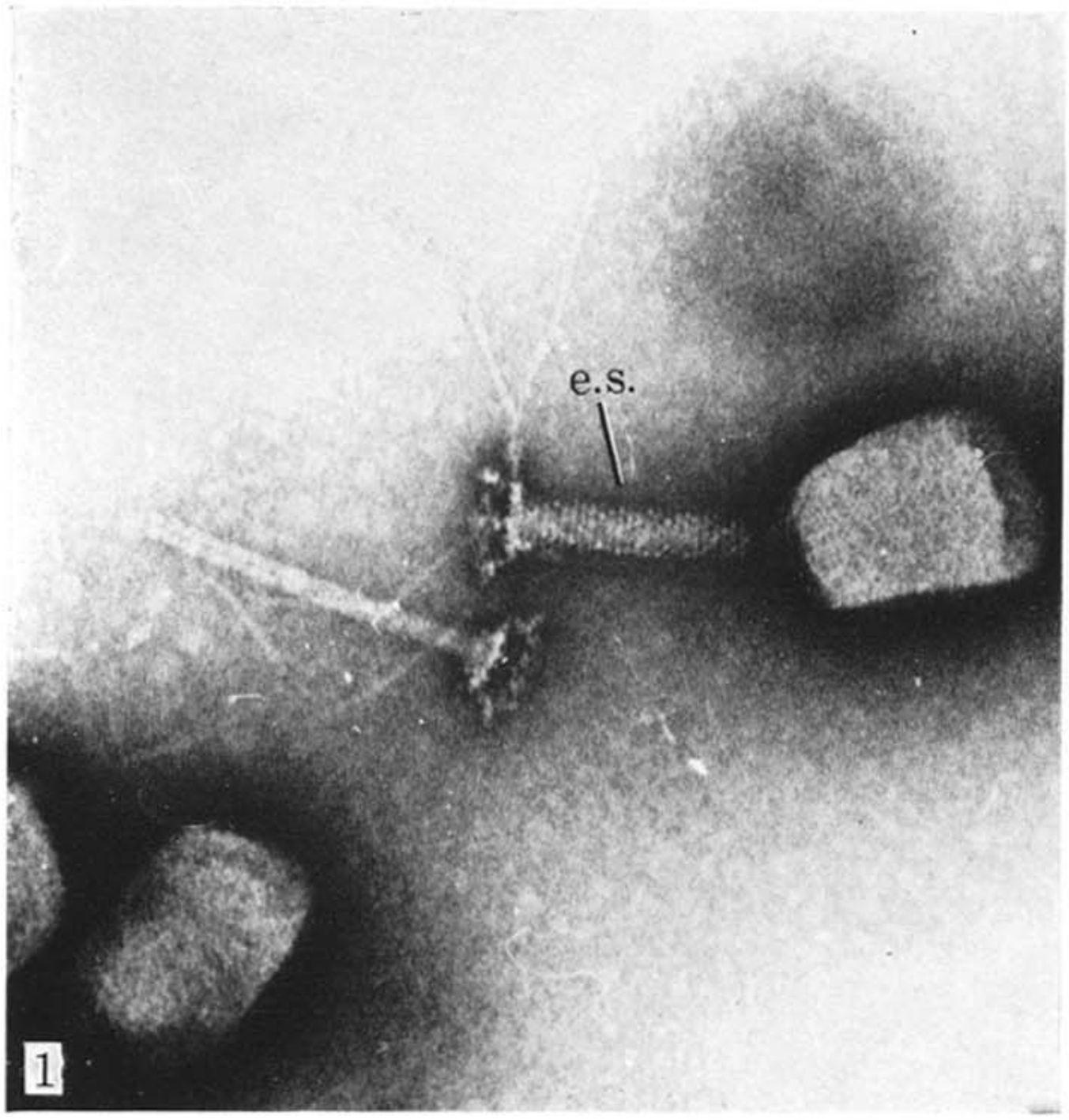

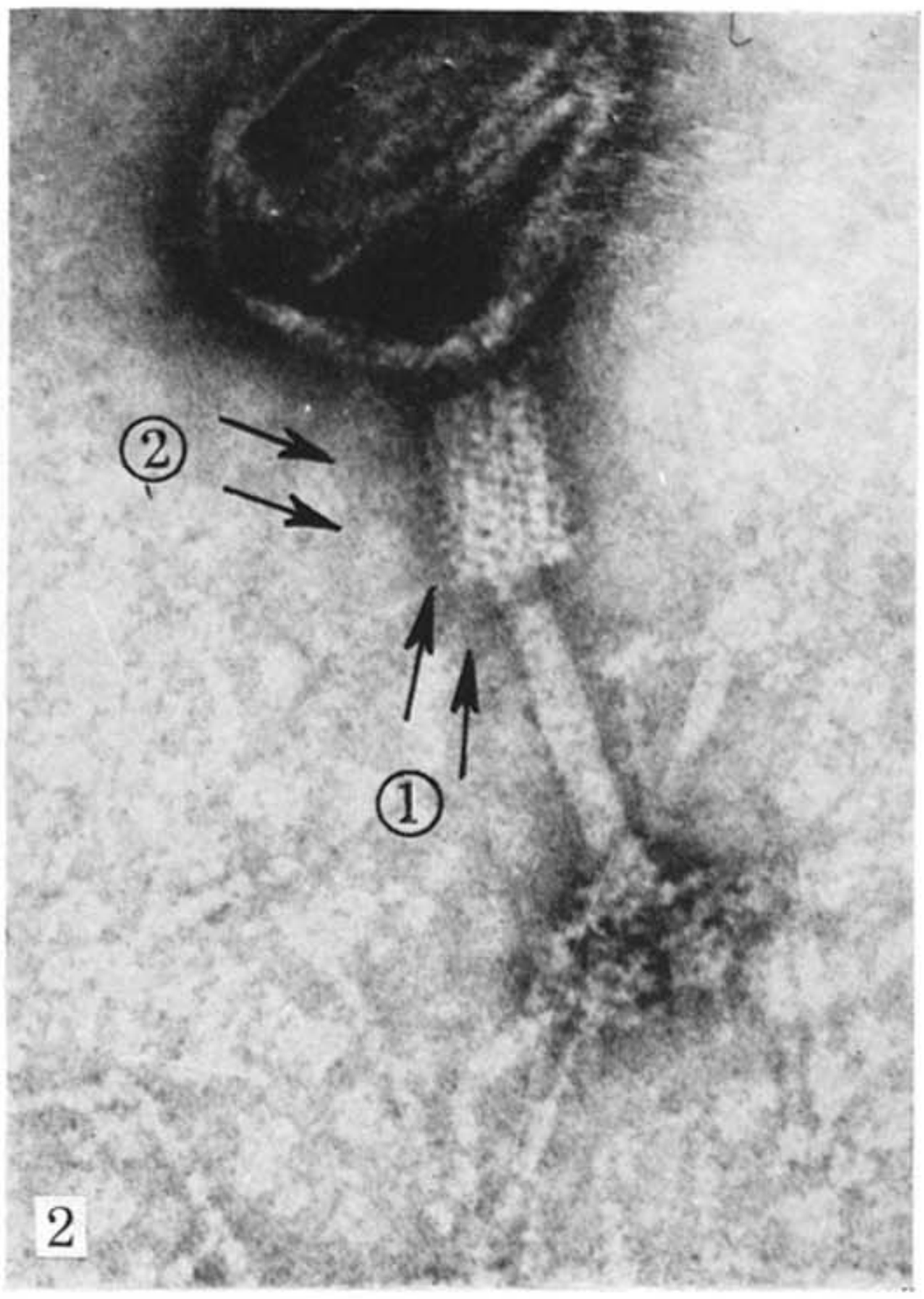

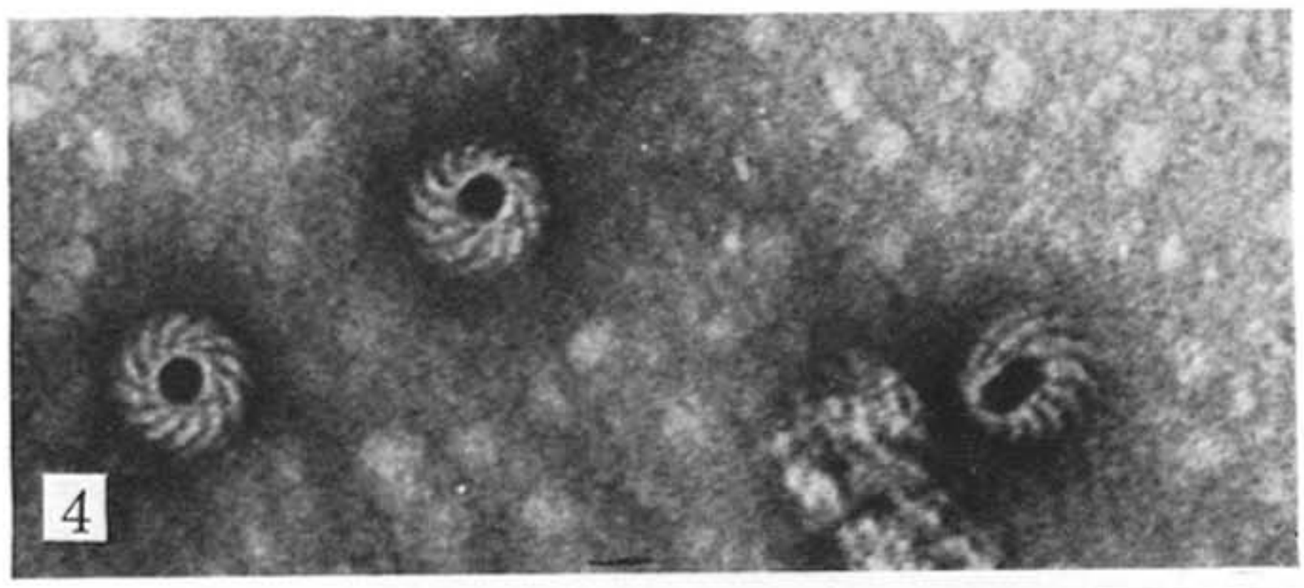

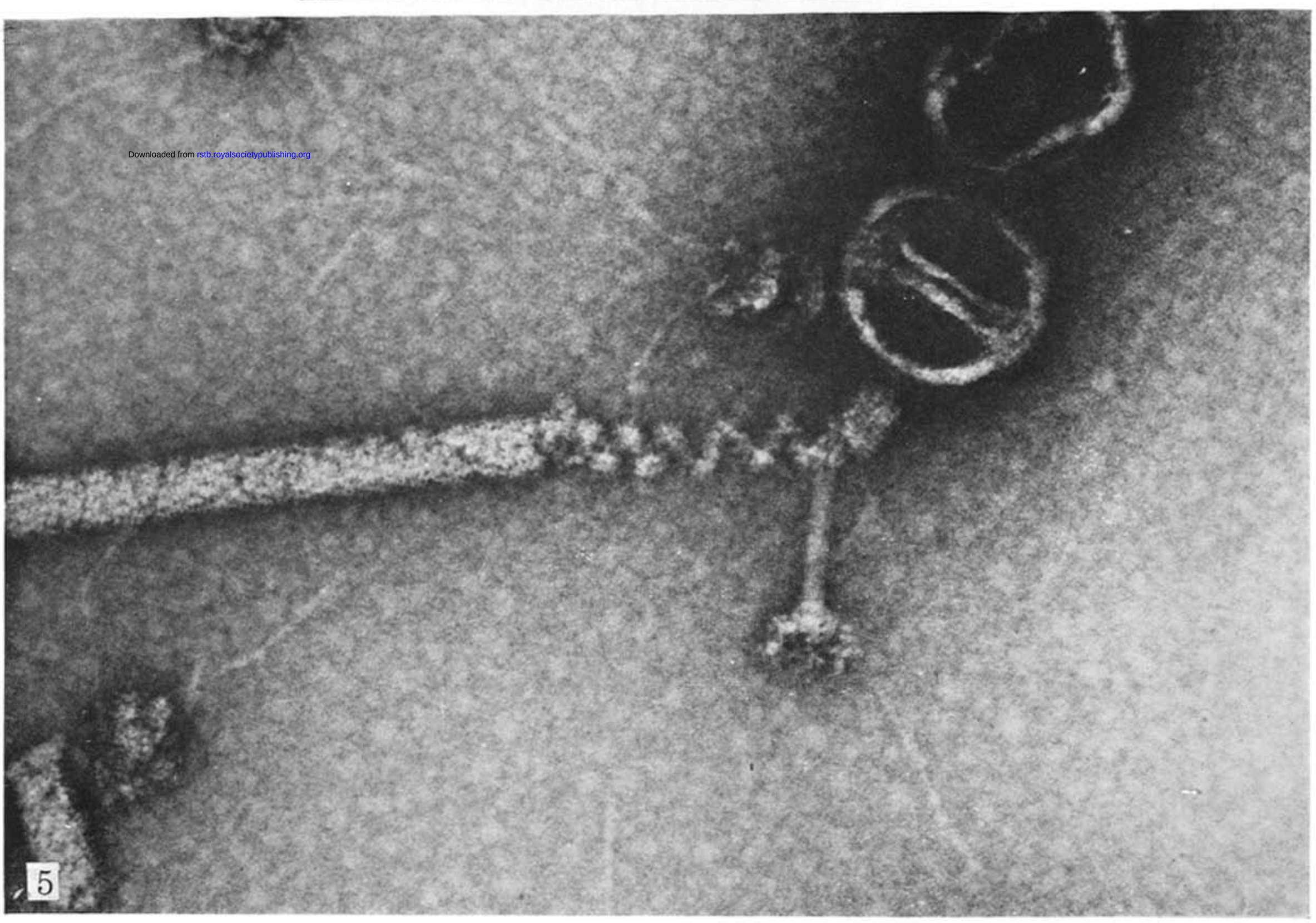

PHILOSOPHICAL TRANSACTIONS OF THE ROYAL SOCIETY B BIOLOGICAL SCIENCES

FIGURES 1, 2, 4 and 5. For legends see facing page.

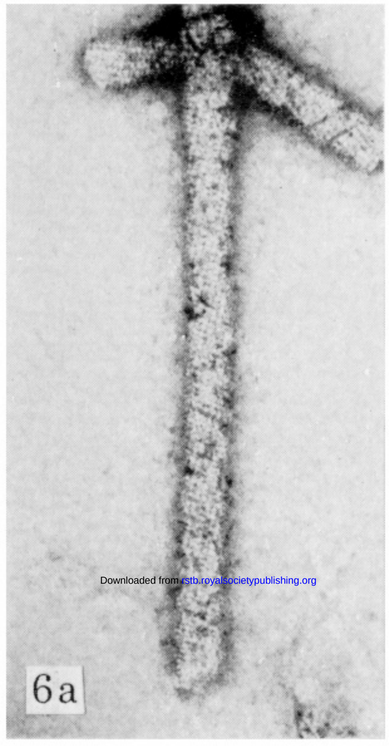

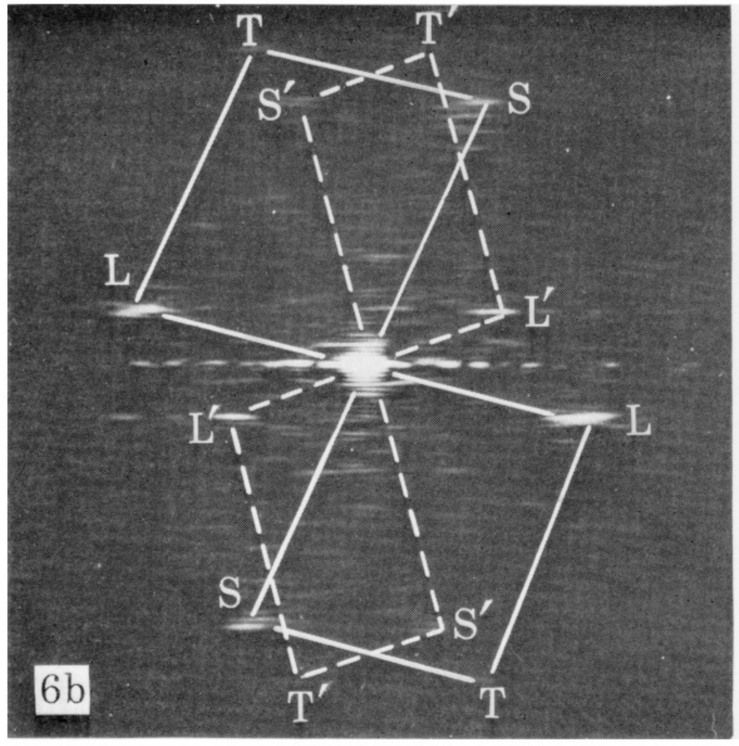

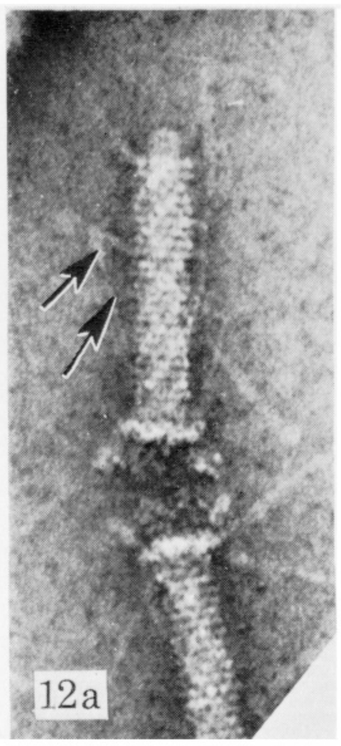

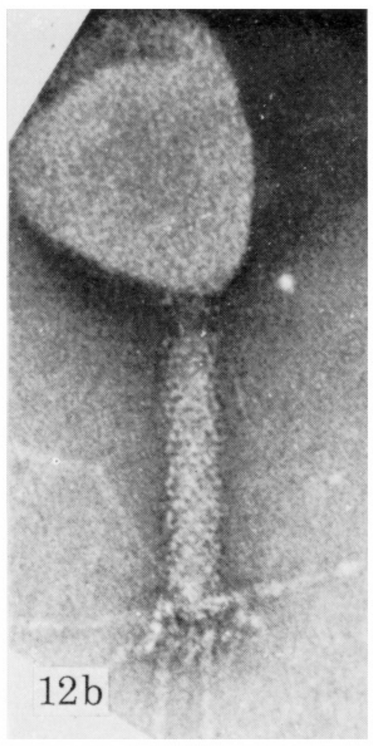

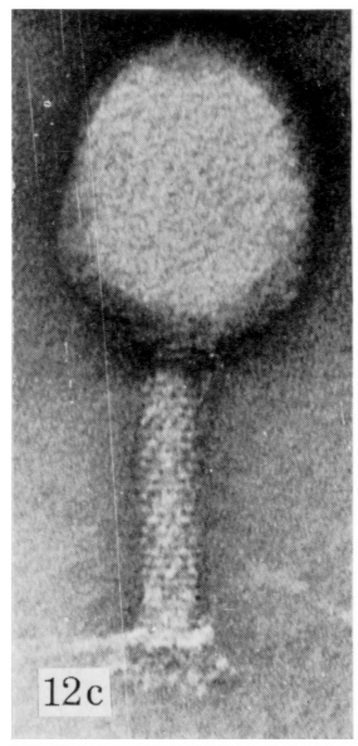

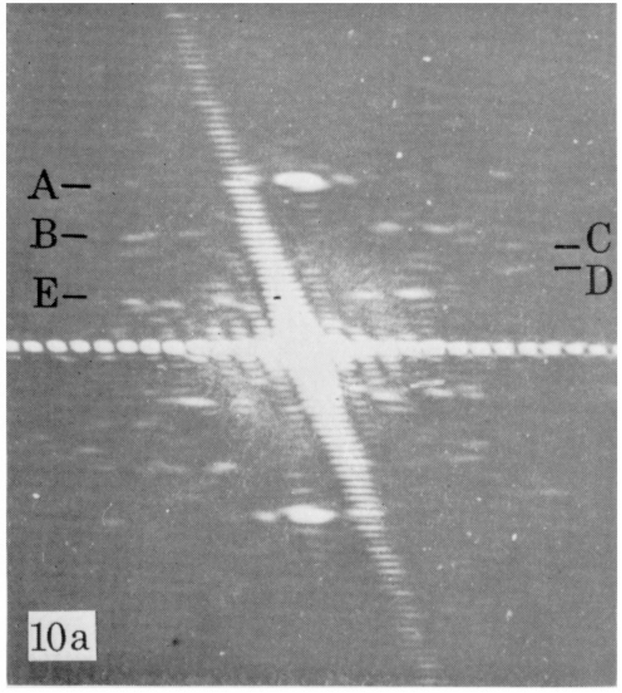

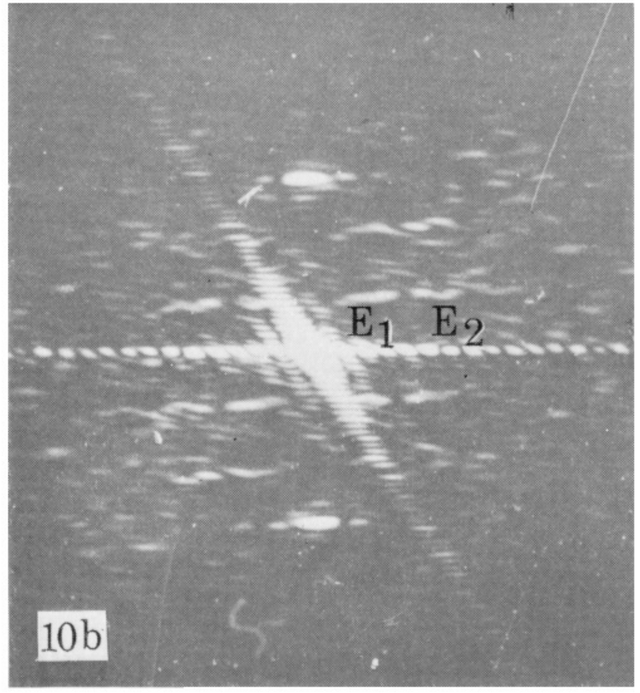

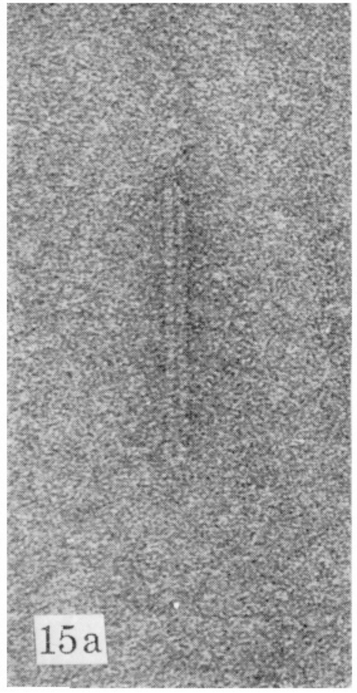

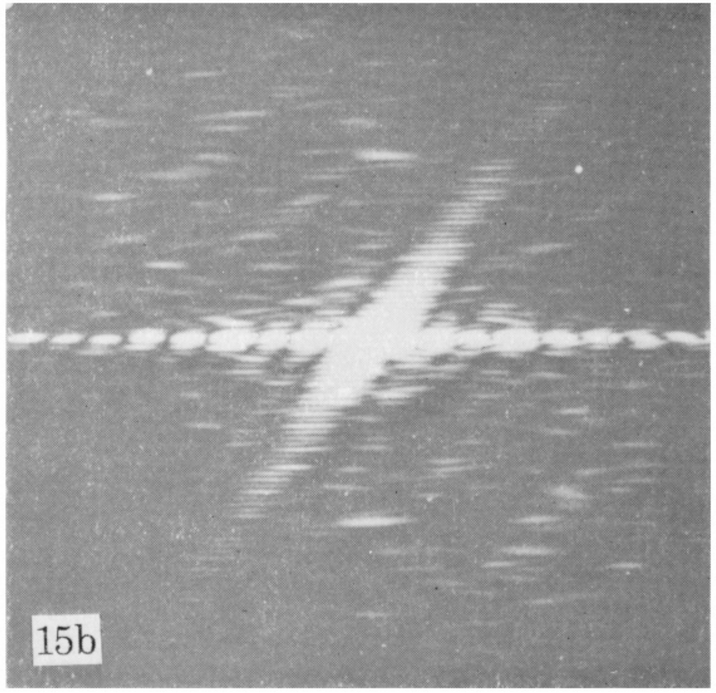

FIGURES 6, 10, 12 and 15. For legends see facing page.